PNAS RESEARCH ARTICLE | IMMUNOLOGY AND INFLAMMATION

The TLR2/TLR6 ligand FSL-1 mitigates radiation-induced hematopoietic injury in mice and nonhuman primates

W. June Brickey[a,b,1], David L. Caudell[c,1], Andrew N. Macintyre[d], John D. Olson[c], Yanwan Dai[e], Sirui Li[b,f], Gregory O. Dugan[c], J. Daniel Bourland[g], Lisa M. O'Donnell[c], Janet A. Tooze[h], Guannan Huang[b,f], Shuangshuang Yang[b,f], Hao Guo[b,f,2], Matthew N. French[d], Allison N. Schorzman[i,3], William C. Zamboni[i], Gregory D. Sempowski[d,4], Zhiguo Li[e,j], Kouros Owzar[e,j], Nelson J. Chao[k], J. Mark Cline[c,5], and Jenny P. Y. Ting[a,b,f,5,6]

Edited by Joel S. Greenberger, University of Pittburgh, Pittsburgh, PA; received December 9, 2021; accepted October 23, 2023 by Editorial Board Member Carl F. Nathan

Thrombocytopenia, hemorrhage, anemia, and infection are life-threatening issues following accidental or intentional radiation exposure. Since few therapeutics are available, safe and efficacious small molecules to mitigate radiation-induced injury need to be developed. Our previous study showed the synthetic TLR2/TLR6 ligand fibroblast stimulating lipopeptide (FSL-1) prolonged survival and provided MyD88-dependent mitigation of hematopoietic acute radiation syndrome (H-ARS) in mice. Although mice and humans differ in TLR number, expression, and function, nonhuman primate (NHP) TLRs are like those of humans; therefore, studying both animal models is critical for drug development. The objectives of this study were to determine the efficacy of FSL-1 on hematopoietic recovery in small and large animal models subjected to sublethal total body irradiation and investigate its mechanism of action. In mice, we demonstrate a lack of adverse effects, an easy route of delivery (subcutaneous) and efficacy in promoting hematopoietic progenitor cell proliferation by FSL-1. NHP given radiation, followed a day later with a single subcutaneous administration of FSL-1, displayed no adversity but showed elevated hematopoietic cells. Our analyses revealed that FSL-1 promoted red blood cell development and induced soluble effectors following radiation exposure. Cytologic analysis of bone marrow aspirates revealed a striking enhancement of mononuclear progenitor cells in FSL-1-treated NHP. Combining the efficacy of FSL-1 in promoting hematopoietic cell recovery with the lack of adverse effects induced by a single administration supports the application of FSL-1 as a viable countermeasure against H-ARS.

radiation | hematopoiesis | animal models | mitigator | innate immunity

Individuals exposed to radiation either from nuclear terrorism or scheduled medical treatment are at risk of developing hematopoietic acute radiation syndrome (H-ARS). Consequences of H-ARS heighten susceptibility to a variety of medical conditions, including anemia, thrombocytopenia, and neutropenia. These patients are prone to hemorrhage, secondary infection, and, subsequently, death. Despite advances in drug discovery aimed to mitigate bone marrow injury, including the application of US Food and Drug Administration (FDA)-approved G-CSF (1), there remains a paucity of therapeutic options available for treating victims of H-ARS.

Hematopoietic stem cells (HSCs) that reside in the bone marrow (BM) of adults give rise to a variety of radiosensitive progenitors and mature cells found in circulation. These include erythrocytes, platelets, and leukocytes that comprise both innate and acquired immune cells. Studies have shown that HSC differentiation and proliferation are regulated through pattern recognition receptors, including Toll-like receptors (TLRs) that signal through downstream transcriptionally activated pathways mediated by the adaptor molecule MyD88 (2) and NF-κB, altering cellular programs of survival, differentiation, migration, and inflammation. Therefore, capitalizing upon the biology of these receptors may prove beneficial to the development of radiation countermeasures targeting cellular responses.

In vivo activation of TLR signaling via treatment with agonists promotes hematopoietic recovery from radiation in mice (3–6). Specifically, we found that mice treated intraperitoneally with the TLR2/TLR6 agonist fibroblast stimulating lipopeptide (FSL-1) following exposure to lethal doses of total body irradiation (TBI) increased recovery of BM and splenic cells (7). FSL-1 has advantages over biologics such as human Growth Hormone (hGH) (8) in that it is a small molecule that is easy to produce and administer. However, to overcome the challenges of species-specific TLR differences between mice and humans (9), incomplete recapitulation of human disease in mouse models, and ethics of testing

Significance

Therapies are needed to address worldwide concerns of nuclear terrorism, accidents, and injuries caused by radiation. We demonstrate that life-threatening hematopoietic injuries in mice and nonhuman primates due to radiation are mitigated with a single subcutaneous administration of the TLR2/TLR6 ligand FSL-1. In mice, bone marrow progenitors are significantly enhanced with FSL-1 treatment after radiation. In nonhuman primates, a single FSL-1 dose after sublethal total body irradiation does not impact physiologic or damage biomarkers, showing lack of adverse clinical effects. Radiation-induced loss of red blood cells is ameliorated by FSL-1 signaling through TLR2/MyD88, up-regulating downstream effector proteins, and promoting hematopoietic cell proliferation. These results indicate that FSL-1 may serve as an effective countermeasure, mitigating radiation-induced hematopoietic injuries.

[1]W.J.B. and D.L.C. contributed equally to this work.

[2]Present address: State Key Laboratory of Cellular Stress Biology, School of Life Sciences, Xiamen University, Xiamen 361102, China.

[3]Present address: BridgeBio Gene Therapy, Raleigh, NC 27607.

[4]Present address: Research Triangle Institute International, Research Triangle Park, NC 27709.

[5]J.M.C. and J.P.Y.T. contributed equally to this work.

[6]To whom correspondence may be addressed. Email: jenny_ting@med.unc.edu.

This article contains supporting information online at https://www.pnas.org/lookup/suppl/doi:10.1073/pnas.2122178120/-/DCSupplemental.

Published December 5, 2023.

radiomitigators in humans, we examined mice as a small animal model and nonhuman primates (NHPs) as a large animal model to advance the preclinical testing of FSL-1.

Cynomolgus (*Macaca fascicularis*) and rhesus (*Macaca mulatta*) macaques share many genetic, physiologic, and anatomic features with humans. As such, TLRs have been widely studied across species including NHPs, humans, and mice, with expression documented in a variety of cell types including myeloid, lymphoid, and epithelial lineages (10, 11). *TLR* expression profiles are strikingly similar between human and NHP (i.e., dendritic cells), whereas many *TLR* patterns are remarkably different between human and mice (12). Notably, *TLR2* and *MYD88* expression profiles show highest abundance in blood and BM in human and NHP as well as in mice (13).

Due to these strong immunological similarities between humans and macaques, NHPs are uniquely valuable for modeling radiation effects and developing radiation countermeasures (14). Our previous work in adult male cynomolgus macaques showed that recombinant hGH mitigated the effects of 2 Gy radiation and enhanced hematopoietic recovery following sublethal whole-body irradiation (8). In the current study, we first verified the dosing and efficacy of FSL-1 in mitigating ARS in mice by stimulating hematopoietic cell proliferation. Then, we applied this knowledge to study the effects of FSL-1 in mitigating the injurious hematopoietic effects of TBI exposure in male rhesus macaques.

Results

To establish preclinical evidence demonstrating the efficacy of FSL-1 as a radiomitigator in animal models, we first performed studies in mice where FSL-1 was administered at 24 h after radiation exposure by a subcutaneous (sc) route, a more acceptable route than intraperitoneal delivery of therapeutics in humans (15). FSL-1 treatment mitigated lethality in C57BL/6 mice treated at 8.2 Gy TBI (Fig. 1*A*), and the more radiosensitive BALB/c strain treated at 7.5 Gy TBI (16, 17) (Fig. 1*B*). Last, FSL-1 improved survival in aged C57BL/6 mice (12 to 18 mo) after 7.5 Gy TBI when FSL-1 was provided sc at 24 h after radiation exposure (Fig. 1*C*). Thus, FSL-1 substantially mitigated radiation lethality in multiple strains and in aged as well as young mice.

To develop FSL-1 as a countermeasure, clinical outcomes were assessed by monitoring changes in body weight and temperature over 30 d following a single administration of increasing FSL-1 doses (5 to 100 μg per dose) in the absence of radiation in C57BL/6 mice. Although treatment to time interactions for weight change with increasing FSL-1 doses were evident, all mice rebounded with weight gain and no mice suffered sustained weight loss (Fig. 1*D*). There were no dose-related changes to body temperature (Fig. 1*E*). Next, we assessed the pharmacokinetics (PK) of FSL-1 (10 to 100 μg or 0.4 to 4.0 mg/kg sc) in naive mice. Blood was collected from mice between 0 and 96 h after FSL-1 administration and processed by mass spectrometry to determine FSL-1 concentration. Maximum FSL-1 plasma concentration was 115 ng/mL at 0.4 mg/kg dosing to 1,338 ng/mL at 4 mg/kg dosing, and the half-life of FSL-1 approximated 3 h (*SI Appendix*, Fig. S1*A*). Radiation (8.2 Gy TBI at 24 h prior to FSL-1 dosing) did not alter the observed half-life of FSL-1 relative to nonirradiated mice (3.2 to 3.4 h; see *SI Appendix*, Fig. S1*B*). These results show no evidence for FSL-1-induced adverse effects in mice.

To assess the impact of FSL-1 on the target receptor TLR2, we examined *Tlr2* mRNA in BM cells collected from mice treated with FSL-1 with and without sublethal irradiation (5 Gy TBI). FSL-1 treatment alone did not affect *Tlr2* expression in naive mice. Expression of *Tlr2* increased in BM cells from WT mice that were given FSL-1 after irradiation, whereas radiation alone in PBS-treated controls did not significantly increase *Tlr2* expression. Control *Tlr2*-deficient mice lacked *Tlr2* induction (Fig. 1*F*). These results suggest a feed forward enhancement of TLR2 by FSL-1 given after radiation.

We and others have shown that TLR2 agonists enhance hematopoietic cell expansion (7, 18). To examine how FSL-1 promotes hematopoietic cells after irradiation, we analyzed BM cells from mice subjected to sublethal irradiation (5 Gy TBI) followed by sc administration of FSL-1 at 24 h post irradiation. First, quantification of $Ki67^+$ (a marker of proliferation) antibody-stained femurs at 8 d after irradiation revealed increased proliferation of hematopoietic cells in BM of unirradiated and irradiated WT mice treated with FSL-1 (Fig. 1 *G* and *H*). FSL-1 promotion of proliferation was dependent on active MyD88 signaling as the proliferative capacity was reduced in FSL-1-treated $Myd88^{-/-}$ mice. Second, immunophenotyping analysis [*SI Appendix*, Fig. S2 *A* and *B* and Table S1 and *Materials and Methods* (19)] of BM cells 8 d after irradiation revealed elevated hematopoietic stem and progenitor cells (HSPC), common myeloid progenitors (CMP), granulocyte-macrophage progenitors (GMP) and megakaryocyte-erythroid progenitors (MEP) following a single FSL-1 dose (+) at 24 h post radiation exposure (Fig. 1 *I–L*). The maturing myeloid cells with $CD11b^+$, $CD11c^+$, $Gr1^+$, and eosinophil markers were enhanced with FSL-1 treatment by 30 d (*SI Appendix*, Fig. S2 *C–F*). In contrast, BM localized maturing subpopulations of $F4/80^+$, $CD3^+$, $B220^+$, and $Ter119^+$ cells were not enhanced with FSL-1 treatment by 30 d (*SI Appendix*, Fig. S2 *G–J*). In addition, the impact of FSL-1 on blood and immune cells in the periphery was examined. Whole blood taken from mice treated without or with radiation plus FSL-1 at days 8 and 30 after treatment was analyzed by clinical chemistry. In unirradiated mice, FSL-1 enhanced platelets. In irradiated mice, slight increases in white blood cells (WBCs) and neutrophils were found at day 8 in FSL-1-treated mice (*SI Appendix*, Fig. S2 *K–P*). Taken together, these results suggest that FSL-1 stimulates the recovery of hematopoietic progenitors, predominantly myeloid cell populations, after radiation exposure in mice. Given these findings in mice, we sought to investigate the role of FSL-1 role in an NHP model.

Initially, we examined the PK of FSL-1 in nonirradiated NHP. This was conducted using appropriate dosing scaled from mice to NHP, based on FDA criteria (20): Three naive NHPs were given a low dose of FSL-1 (0.03 mg/kg) and another three were given a higher FSL-1 dose (0.09 mg/kg). Blood samples were collected serially from treated NHP over a span of 0 to 72 h and then analyzed by LC-MS/MS for FSL-1 plasma content (*SI Appendix*, Fig. S3*A*). The single administration of FSL-1 (0.09 mg/kg) produced a maximum plasma concentration of 116 ng/mL with a 14.2 h half-life, longer than previously observed in mice.

To test the radiomitigation capacity of FSL-1 in NHP, monkeys were given sublethal TBI (4 Gy) followed by a single sc administration of FSL-1 (0.09 mg/kg) 24 h later. This dose is the maximum allowed by the animal protocol. An experimental strategy was designed to satisfy power calculations and practical considerations for handling the monkeys with 10 NHPs in each FSL-1 and Vehicle (PBS) control cohort. This supported treatment, monitoring, and sample collection of NHP and balanced for age and body weight (*SI Appendix*, Fig. S3 *B* and *C*).

Multiple parameters were followed to assess clinical outcomes of irradiated NHP with and without FSL-1 administration. FSL-1-treated NHP showed slightly more weight loss during the monitoring period ($P = 0.0095$, Fig. 2*A*), but this did not pose a clinical concern. The lack of body temperature change suggested no evidence of adverse effects caused by FSL-1 (Fig. 2*B*). Likewise, physiologic biomarkers blood glucose, heart rate, respiration, mean arterial

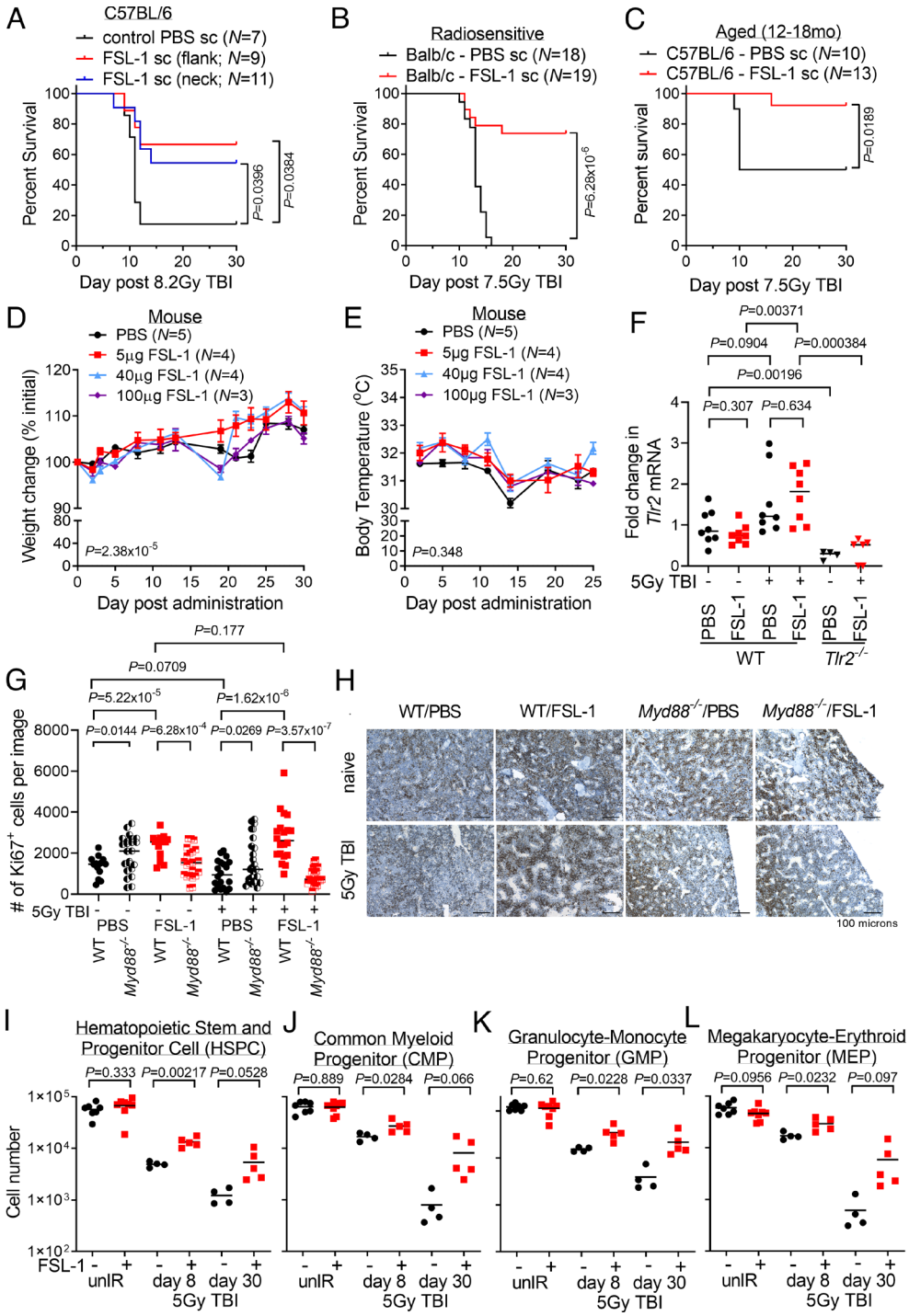

Fig. 1. FSL-1 effectively mitigated acute radiation-induced lethality in mice by minimizing adverse effects and enhancing proliferation of hematopoietic progenitor cells. (*A*) C57BL/6 mice were administered FSL-1 subcutaneously (sc) in abdominal flank or scruffed neck 24 h after 8.2 Gy TBI. (*B*) Balb/c mice were administered FSL-1 (sc) at 24 h after 7.5 Gy TBI. (*C*) Aged C57BL/6 mice (12 to 18 mo) were given FSL-1 (sc) after 7.5 Gy TBI. Survival distributions in Kaplan–Meier plots and log-rank test *P* values are shown. Investigating adverse effects, naive mice were given a single FSL-1 sc injection (5 to 100 µg), and changes in weight (*D*) or body temperature (*E*) were monitored with mean ± SEM shown from a representative experiment of three replicate studies. Repeated measurements were assessed using linear mixed-effects modeling with *P* values for treatment to time interaction indicated. (*F*) qPCR studies were conducted to assess *Tlr2* mRNA in bone marrow (BM) cells from WT and $Tlr2^{-/-}$ mice treated with radiation (5 Gy TBI) with (+) and without (−) FSL-1. (*G* and *H*) Femur tissue sections prepared at day 8 post treatment were probed with Ki67 antibodies, imaged and proliferating cells were quantified using ImageJ. Scale bar at 100 µm shown on representative images. Pairwise *t* tests (unpaired data, unequal variance, two-sided) were applied with *P* values shown and mean indicated by bar. (*I*) BM hematopoietic stem and progenitor cells (HSPCs), (*J*) common myeloid progenitors (CMPs), (*K*) granulocyte-macrophage progenitors (GMPs), and (*L*) megakaryocyte-erythroid progenitors (MEPs) in unirradiated (unIR) and irradiated mice BM harvested on days 8 and 30 after PBS or FSL-1 sc injections on day 1 were immunophenotyped by flow cytometry. Two-sample *t* tests were performed for unpaired BM cell data with Welch's approximation assuming variance between treatment groups. *P* values are indicated. Each symbol represents an individual mouse (*F* and *I*–*L*) or image of fixed bones (*G*).

pressure, and pulse oximetry did not differ between the cohorts over the course of the study (Fig. 2 *C*–*E* and *SI Appendix*, Fig. S3 *D* and *E*). Renal biomarkers blood urea nitrogen (BUN) and creatinine diminished after irradiation, but serum levels in FSL-1- vs. PBS-treated NHP were not different (Fig. 2*F* and *SI Appendix*, Fig. S3*F*). Other tissue damage biomarkers, including total serum protein, the albumin/globulin ratio, and alkaline phosphatase, did not deviate for 65 d between the FSL-1- and Vehicle-treated cohorts (Fig. 2*G* and *SI Appendix*, Fig. S3 *G* and *H*). Hepatic biomarkers alanine transaminase (ALT) and aspartate transaminase (AST) were not different between cohorts (Fig. 2 *H* and *I*). Furthermore, the bicarbonate, chloride, and calcium serum levels did not differ (*SI Appendix*, Fig. S3 *I*–*K*). Few NHPs developed short-term diarrhea that occurred at a similar rate between cohorts (Fig. 2*J*); a single FSL-1-treated animal was an outlier with more frequent diarrhea. Cutaneous bruising or microhemorrhaging seen in NHP was minimal, similar between the cohorts, and attributed to venipuncture (Fig. 2*K*). Last, NHPs were followed for up to 850 d, and blood sample analyses between treatment cohorts showed no differences in adverse clinical markers of body weight, total serum protein, albumin/globulin, aspartate transaminase, or BUN, with the only exception being alkaline phosphatase that differed between cohorts but remained within normal reference range (*SI Appendix*, Fig. S4 *A*–*F*). Taken together, these observations demonstrate that a single administration of FSL-1 after radiation exposure produced no clinical evidence of adverse effects in NHP.

TLR agonists and growth factors have demonstrated mitigating effects against H-ARS after radiation exposure (7, 21–24). To

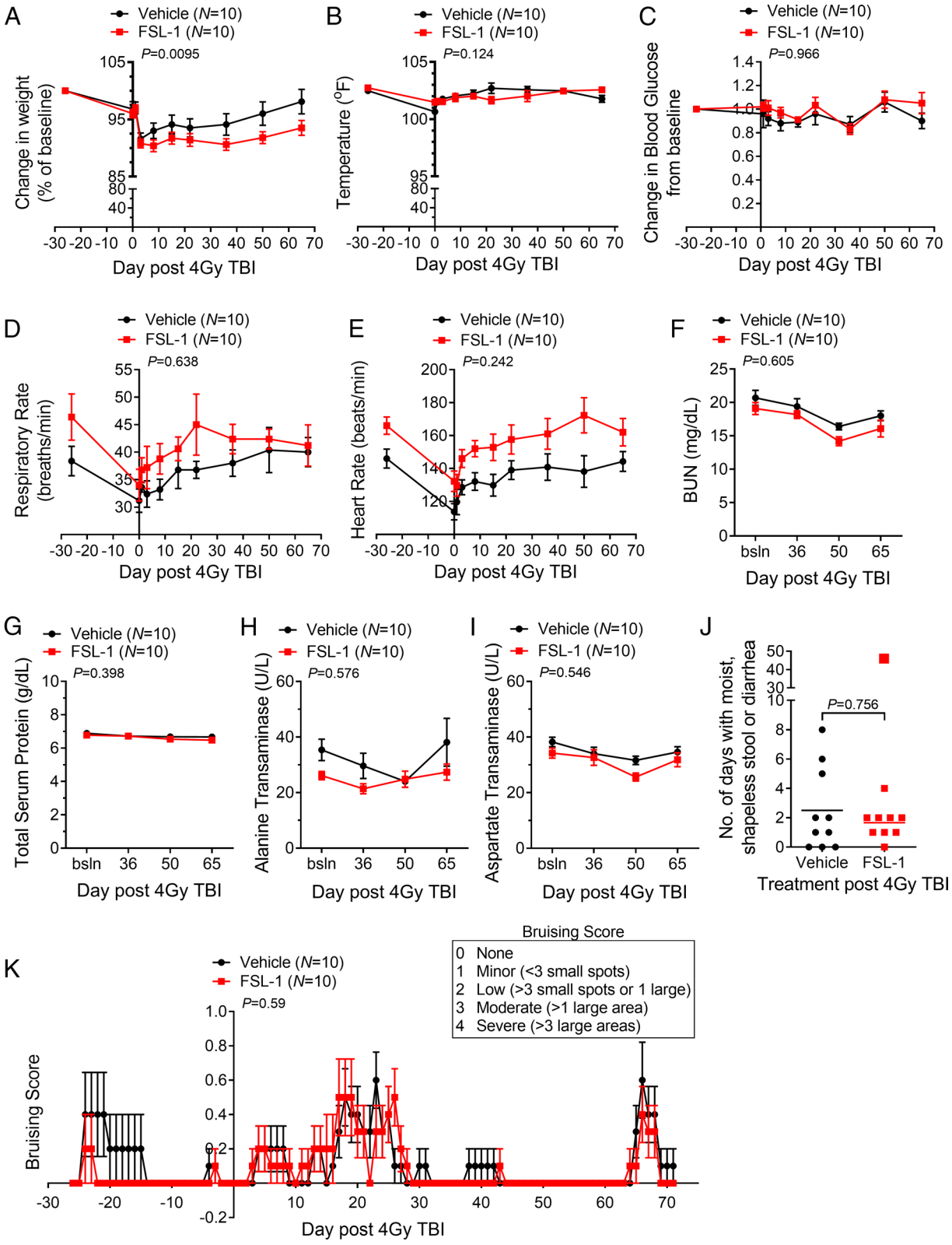

Fig. 2. Nonhuman primates (NHPs) given sublethal total body irradiation followed by one subcutaneous administration of FSL-1 showed few clinical signs of adversity. NHPs were subjected to 4 Gy TBI and given FSL-1 or Vehicle injections (sc) 24 h later. (*A*) Changes in body weight relative to baseline weight (%) and (*B*) body temperatures (°F) are indicated. The physiologic measures of blood glucose change (*C*), respiratory rate (*D*), and heart rate (*E*) are indicated. Injury markers in peripheral blood, including blood urea nitrogen (BUN) (*F*), total serum protein (*G*), alanine transaminase (*H*), and aspartate transaminase (*I*), are shown. Longitudinally repeated blood chemistry and physiologic measures were assessed by linear mixed-effects models. All pretreatment values were considered baseline and used as covariates in the mixed-effects models, with treatment over time *P* values shown (*A*–*E*). For variables that indicated baseline categorically, a linear mixed-effects regression model was augmented with a fixed additive effect for the baseline value along with first- and second-order interaction terms (*F*–*I*). (*J*) Softened stool or diarrhea over a span of 3 successive days was monitored. The outlier with 48 d of softened stool in the FSL-1 cohort is shown, but not included in statistical analysis. Since the assumption of normality was not appropriate based on the distribution, the Wilcoxon rank-sum test was applied to unpaired data, and asymptotic *P* value is reported. Incidences of bruising (*K*) are presented based on subjective scoring as shown in the box. The ordinal logistic regression model including additive fixed effects for time, treatment, and their interaction was applied to analyze treatment on bruising over time. Each Vehicle- and FSL-1-treated cohort are composed of *N* = 10 NHP with mean ± SEM shown (*A*–*I*, and *K*), or each symbol represents an individual (*J*).

measure the function of FSL-1 in reducing hematopoietic dysfunction in NHP, a complete blood cell count (CBC) was conducted on peripheral blood samples collected from monkeys prior to treatment and then at various times following irradiation through 65 d. Identifying the nadir at day 15, the CBC data between the cohorts was analyzed before this point as injury (pre) and after this point (post) as recovery. The attenuated loss of erythrocytes (RBC), hematocrit, and hemoglobin improved recovery in FSL-1-treated NHP (linear mixed-effects model post nadir treatment, $P \leq 0.01$; Wilcoxon test for day 15 through day 65 treatment, $P < 0.05$) (Fig. 3 *A*–*C*). The decline in platelets (PLT) in FSL-1-treated NHP did not reach the same nadir as Vehicle controls (Wilcoxon test for day 15 treatment, $P = 0.0375$); both cohorts showed a similar rebound in PLT during recovery (Fig. 3*D*). Monocytes appeared to rapidly recover after the nadir point (Wilcoxon test for day 15 through day 65 treatment, $P = 0.064$) with FSL-1 treatment (Fig. 3*E*). Extended monitoring of circulating blood cells through 600 d after treatment revealed a sustained elevation of RBC and hemoglobin with FSL-1 treatment after day 16 (*SI Appendix*, Fig. S4 *G* and *H*). In contrast, white blood cells (WBCs), PLT, neutrophils, and monocytes (MC) in the blood decreased after irradiation but did not differ between treatment cohorts (*SI Appendix*, Fig. S4 *I*–*L*). Overall, enhancement of RBC recovery shows the benefit of FSL-1 treatment to overcome acute and chronic anemia from radiation exposure.

The effects of TBI are often accompanied by changes in serum proteins; thus, we investigated these factors in peripheral blood samples using a multiplex panel of 23 cytokines. Although there were no significant differences in factors between FSL-1 vs. Vehicle groups, changes in serum G-CSF, IL-13, IL-15, and MCP1 ($P = 0.057$, baseline to day 50) were observed (*SI Appendix*, Fig. S5). We note a progressive decline in sCD40L levels ($P = 0.087$ for baseline to day 50), a trend toward reduction in MIP1a from baseline through day 15 ($P = 0.078$), IFNγ baseline through day 8 ($P = 0.064$), and in IL-8 baseline through day 50 ($P = 0.064$). These findings are consistent with previous studies linking these factors to radiation and/or subsequent NF-κB activity and support TLR2-mediated impacts on cell migration, differentiation, and tissue repair programs (25, 26). No differences with respect to treatment were found in other analytes (i.e., IL-1ra, IL-10, IL-12/23, IL-1β, IL-2, IL-4, IL-5, IL-17A, GM-CSF, TGFa, VEGF, MIP1b) or inflammatory factors induced by NF-κB (i.e., IL-6, IL-18, TNF) (27–29) (*SI Appendix*, Fig. S5). Irradiated NHP treated with FSL-1 had lower total monocytes circulating during the first 3 d after irradiation, followed by greater recovery of monocytes and plasmacytoid DC (*SI Appendix*, Fig. S6). Lymphocyte populations did not vary between cohorts (*SI Appendix*, Fig. S6) (30, 31). These results show minimal or transient impact of FSL-1 on circulating leukocytes.

Given the findings in mice that showed enhanced hematopoietic progenitor proliferation, we sought to determine the effects of FSL-1 on NHP hematopoietic progenitor development. BM aspirates from treated NHP collected at baseline, day 22 (near nadir) and day 65 (recovery) had abundant cellularity in FSL-1-treated NHP at day 22, near to the nadir after irradiation, whereas Vehicle-treated specimens were markedly hypocellular, an outcome attributed to radiation injury (Fig. 3*F*). Of note, there were increased erythroid cells in the FSL-1-treated samples, suggesting a protective effect by FSL-1 on erythroid precursors during the injury phase (baseline to day 22, $P = 0.035$) (Fig. 3*G*), with a less pronounced drop in precursors from baseline to day 22. This pattern of reduction by day 22 in other precursor populations in Vehicle controls appeared greater than in FSL-1-treated subjects, but changes in abundance were not statistically different (Fig. 3 *H*–*L*). No statistical differences between cohorts were found for recovery from day 22 to day 65. However, monocyte (MC) precursors at day 65 in FSL-1-treated NHP were significantly ($P = 0.048$) restored to baseline levels whereas MC precursor restoration lagged in controls (Fig. 3*J*). These data reflect the activity of FSL-1 in promoting hematopoietic progenitor cell recovery after radiation injury, especially RBC and MC in NHP.

To decipher the mechanism of action of FSL-1 in mitigating H-ARS, factors activated by the TLR2/TLR6 pathway were investigated using approaches to analyze RNA and protein in BM samples collected from treated mice and NHP. First, since radiation creates cell damage and death, we investigated how FSL-1 impacts a damage marker by measuring phosphorylated γ-H2AX in mouse BM cells by immunoblotting of day 8 after irradiation lysates. Radiation exacerbated H2AX levels as seen in PBS treated irradiated mice over unirradiated mice ($P = 0.0331$), whereas FSL-1 treatment produced no differences (*SI Appendix*, Fig. S7 *A* and *B*). Additionally, cell death in femur sections prepared from irradiated and treated mice was assessed histologically at day 8 by staining with TUNEL reagent (Fig. 4 *A* and *B*). As expected, $TUNEL^+$ cell numbers were elevated with radiation injury ($P < 0.00002$). FSL-1 treatment significantly diminished the number of $TUNEL^+$ cells in unirradiated mice ($P = 0.0133$) and with radiation ($P = 0.004$). These results suggest a protective anti-death role for FSL-1 when given after radiation, possibly mediated through NF-κB activation.

Second, expression of immune, inflammatory, and cell differentiation markers activated by TLR2 signaling was examined. Changes in *Mmp9* mRNA in mouse BM cell harvested at day 8 after 5 Gy TBI were determined by qPCR, as MMP9 is an important cell and tissue reprogramming factor and has been shown previously to be induced by TLR5 activation in the context of radiation (32) and FSL-1 stimulation in the context of human monocytic cells (33). In the absence of radiation, FSL-1 significantly increased *Mmp9* expression ($P = 0.0103$), and this dependence on TLR2/MyD88 activation was validated in $Myd88^{-/-}$ mice (Fig. 4*C*, $P \leq 0.01$). However, in the presence of radiation, *Mmp9* expression in FSL-1-treated mice did not differ from levels in PBS-treated mice and remained MyD88-dependent (Fig. 4*C*). For NHP, intact total RNA isolated from four cryopreserved BM aspirates of either Vehicle- or FSL-1-treated NHP cohorts was subjected to NanoString RNA nCounter profiling (34). For FSL-1- vs. Vehicle-treated NHP samples, we observed differences in expression from baseline to day 22 in *TLR2* and *TLR6* transcripts; from baseline to day 65 in *TLR2*, *TLR6, CASP3,* and *TNF* transcripts; and from day 22 to day 65 in *TLR2*, *TLR6, MyD88,* and *CASP3* transcripts (Fig. 4 *D*–*H*). There were no differences in *MMP9* expression between FSL-1- and Vehicle-treated cohorts (Fig. 4*I*). These results suggest that activation of innate immune gene expression with FSL-1 treatment supports a BM niche conducive to hematopoiesis.

Finally, we investigated MAPK p38 activation as a biomarker for mediating TLR2/MyD88 signals (33, 35) as previously shown in reports of FSL-1 activating p38 MAPK and NF-κB in a MyD88-dependent manner in melanocytes, keratinocytes, monocytes, or fibroblasts (33, 36–38). BM cell lysates prepared from mice treated with radiation and/or FSL-1 were probed using antibody-targeted immunoblotting against activated phosphorylated (P-) and total p38 MAPK. Radiation diminished P-p38 levels ($P = 0.0177$), whereas P-p38 levels in FSL-1-treated unirradiated compared to irradiated were unaltered (*SI Appendix*, Fig. S7 *A* and *C*). The single time point of 8 d after treatment and heterogeneous BM populations may be inappropriate to show FSL-1 activation of p38 MAPK. These biomarker studies

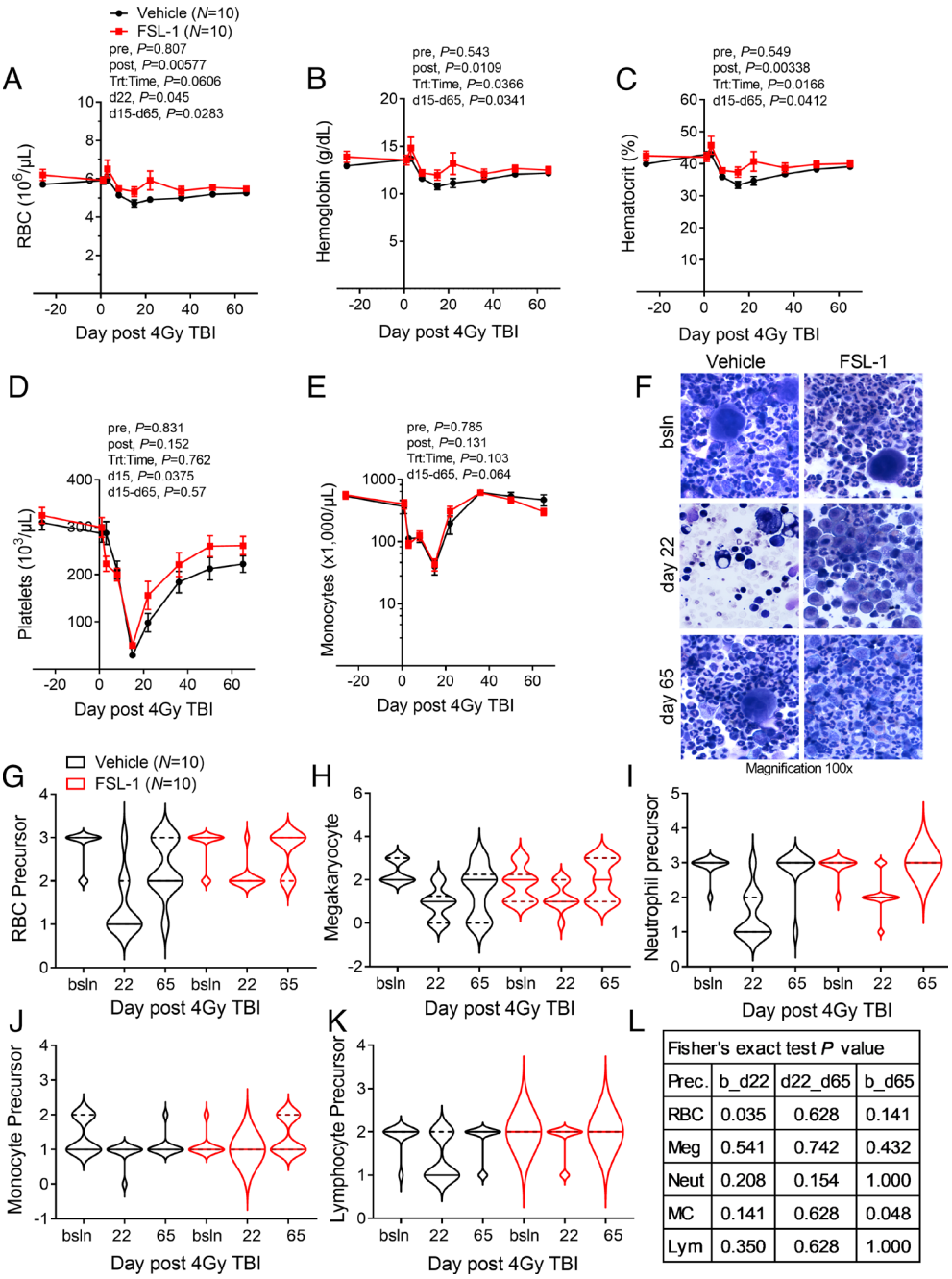

L

Fisher's exact test *P* value			
Prec.	b_d22	d22_d65	b_d65
RBC	0.035	0.628	0.141
Meg	0.541	0.742	0.432
Neut	0.208	0.154	1.000
MC	0.141	0.628	0.048
Lym	0.350	0.628	1.000

Fig. 3. FSL-1 enhanced hematopoietic cell recovery in the periphery and bone marrow of irradiated NHP. Peripheral blood and BM samples were collected before radiation, at treatment, and at selected times for 65 d after radiation. Blood constituents were analyzed by hematologic assays, enumerating red blood cells (RBCs) (*A*), hemoglobin (*B*), hematocrit (*C*), platelets (*D*), and monocytes (*E*). For (*A*–*E*), mean ± SEM is shown (*N* = 10/cohort), where lines connect means across time points. Repeated measurements were evaluated using linear mixed-effects models, except where the fitted linear mixed-effects model was singular, such that a Bayesian linear mixed-effects model was implemented pre and post the nadir (at day 15) (*A*–*E*). As turning points were detected along the time, linear mixed-effects models were fit before (pre) and after (post) the detected turning time (nadir), with baseline as a fixed additive effect for prenadir models. *P* values for treatment pre/post nadir and for treatment to time interaction post nadir are indicated. Wilcoxon rank-sum testing was performed between Vehicle and FSL-1 treatment cohorts for measures on selected times (days d15 or d22) or for time period (d15 to d65), with indicated *P* values. (*F*) BM aspirates from FSL-1- or Vehicle-treated NHP at baseline (bsln) and days 22 and 65 after radiation were stained with Diff-Quik, with representative images at magnification of 100× under oil immersion for each cohort (*N* = 10) displayed. Abundance of cell types was tallied in a blinded fashion based on a scale from 0 (none) to 3 (most abundant). The violin plots reflect the abundance of precursor subpopulations with medians shown as solid bars and quartiles indicated by dashed bars for (*G*) RBC, (*H*) platelets (megakaryocytes), (*I*) neutrophils, (*J*) monocytes, and (*K*) lymphocytes. (*L*) Abundance changes between time points for Vehicle- vs. FSL-1-treated cohorts were evaluated using Fisher's exact tests, with *P* values indicated (bsln or b to d22, d22 to d65 and b to d65).

lead to a proposed model whereby FSL-1 binds TLR2/TLR6, triggering intracellular pathways and inducing transcriptional regulation of specific cytokines and growth factors that are employed by the BM niche to promote hematopoiesis (Fig. 4*J*). In summary, we find enhanced recovery of hematopoietic progenitors, especially erythroid and myeloid lineages, in FSL-1-treated irradiated subjects. These results indicate that FSL-1 mitigates radiation-induced hematopoietic injury in both mice and NHP and thereby supports FSL-1 as a viable candidate for further development as a medical countermeasure.

Discussion

This proof-of-concept study was performed in both mice and NHP. The studies informed the feasibility of a subcutaneous FSL-1 injection, the lack of adverse effects, the promotion of hematopoietic recovery in two animal models, and, thus, compliance with the US FDA two-animal rule for developing human therapeutics. Studying these nonterminal animal models using physical and clinical evaluations including serum chemistry of hepatic and renal function, we showed that FSL-1 caused no long-lasting adverse clinical effects. Following subcutaneous administration of the mitigator at 24 h after irradiation, Vehicle-treated NHP gained more weight, starting at day 20 in contrast to ~day 35 for FSL-1-treated subjects. Despite the difference between the two groups of NHP during the 65-d study period, the difference in weight gain never reached clinical or regulatory concerns and was indistinguishable by ~800 d after treatment, even though the NHP had been housed in different environments after the 65-d study. Similarly, weight and temperature loss attributed to increasing FSL-1 dosing was transient in mice with no adverse effects.

The mechanisms by which TLR signaling regulates the proliferation and differentiation of HSC are under intense investigation, with most studies examining cellular responses in vitro (39–41).

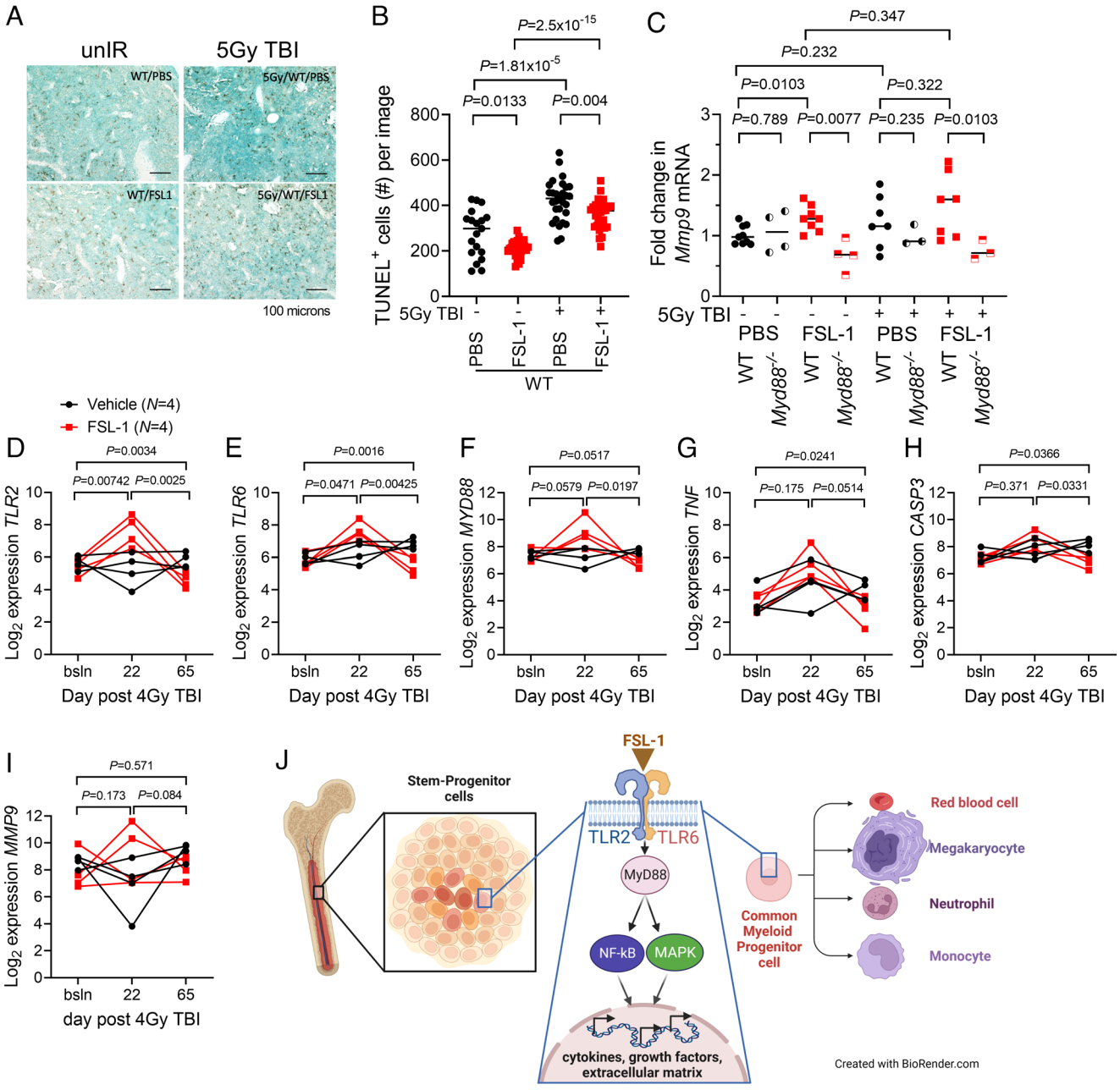

Fig. 4. FSL-1 stimulated TLR2/TLR6 signaling and activated downstream transcriptional regulation. (*A*) TUNEL immunohistochemistry of murine femur sections was conducted to study cell death. Femur tissue sections prepared from treated C57BL/6 mice on day 8 after radiation were probed with TUNEL HRP reagent. The scale bar is 100 μm. (*B*) Quantitation of number (#) of TUNEL$^+$ cells per image was conducted using ImageJ, with each symbol representing an individual femur sample. Statistical significance was determined using pairwise *t* tests, with *P* values indicated. (*C*) *Mmp9* mRNA from BM cells harvested at 8 d from FSL-1-treated control and irradiated mice was quantified by qPCR analysis. Each symbol represents an individual mouse with bar indicating the mean. Data (unpaired, unequal variance, two-sided) were evaluated using *t* tests (unpaired data), with *P* values indicated. (*D–I*) Transcript profiling of NHP RNA was conducted on BM biopsies from Vehicle ($N = 4$) and FSL-1 ($N = 4$) treated irradiated NHP using NanoString technology. String plots for differentially expressed genes (*TLR2*, *TLR6*, *MyD88, TNF, CASP3*, and *MMP9)* are shown, where connected lines between symbols represent an individual NHP. The *t* test (unpaired data) was used to decipher changes in transcripts between FSL-1 and Vehicle treatments at bracketed time points between bsln to d22, d22 to d65 or bsln to d65. (*J*) A mechanism is proposed whereby FSL-1 binds TLR2/TLR6, resulting in activation of MyD88, NF-κB, and MAPK activities, and culminating in transcriptional regulation of cytokines, growth factors, and extracellular matrix components that promote proliferation of hematopoietic progenitors.

Generally, during hematopoietic stress, injury, or infection, the BM responds through proliferation of leukocyte progenitors that ultimately enter circulation and respond to injury through a programmed inflammatory process. Herman et al. showed that activation of TLR2 results in expansion of the HSC pool in a G-CSF-mediated manner (18). Our previous study in mice demonstrated that FSL-1 mitigates radiation injury through the MyD88 complex (7). Here, testing NHP confirmed the earlier and current mice studies that TLR2/TLR6 signaling activation is correlated with induced BM progenitor cell proliferation in response to radiation injury, especially among RBC and monocyte precursors.

Following radiation exposure, FSL-1 treatment induced changes in hematopoietic responses. First, FSL-1 enhanced the reconstitution of BM cellularity in FSL-1-treated NHP by day 22. Second, hematopoietic progenitors in FSL-1-treated irradiated mice displayed greater proliferation at day 8 than found in non-FSL-1-treated mice. Third, radiation-induced reductions of

RBC mass in the erythron, including RBC count, hematocrit, and hemoglobin, recovered more rapidly in FSL-1-treated NHP compared to controls, alleviating anemia (42, 43). Finally, evaluation of key regulatory factors (TNF, G-CSF, and MMP9) may indicate hematopoietic cell recovery is influenced by TLR2 activation (44–46).

In summary, these data show that a single sc administration of FSL-1 given 1 d after radiation exposure mitigates anemia caused by sublethal radiation exposure in NHP. In mice, we observed an enhancement of RBC, megakaryocytes, and myeloid progenitors. The differences may be attributed to the higher dose of radiation used in mice compared to NHP, species differences in hematopoietic niche crosstalk or in species-related drug metabolism. Nonetheless, this study in NHP extends our findings based on the hematopoietic progenitor cell promoting activity of FSL-1 against H-ARS shown in mice. Taken together, these results indicate that this TLR2/TLR6 ligand may serve as an effective mitigator of H-ARS.

Materials and Methods

Mice. The mice including male and female, aged 8 to 16 wk or 12 to 18 mo, for these studies were obtained from Jackson Research Labs or bred in-house at the University of North Carolina at Chapel Hill. The mouse strains included C57BL/6, BALB/c, *Myd88*$^{-/-}$, and *Tlr2*$^{-/-}$. Mice were housed under specific pathogen-free conditions in cages with autoclaved corncob bedding, fed autoclaved extruded chow (LabDiet, Purina 5V0F/G), and given access to autoclaved water ad libitum. Animal facilities have been accredited by the Association for Assessment and Accreditation of Laboratory Animal Care, International (AAALAC). All procedures were approved by the Institutional Animal Care and Use Committee (IACUC) of the University of North Carolina at Chapel Hill, NC.

Nonhuman Primates. Twenty-six male rhesus macaques (*Macaca mulatta*; $N = 20$ irradiated and $N = 6$ nonirradiated controls) were studied, ranging in age (4.5 to 8 y) and in weight (5 to 15 kg), but matched between Vehicle- and FSL-1-treated groups. The control and irradiated NHP were obtained from Wake Forest University (Winston Salem, NC) and Primate Products, Inc. All blood collections and other post-irradiation procedures were conducted at the Wake Forest University School of Medicine (WFSM) with approval by of the Wake Forest University IACUC. WFSM is committed to providing a high-quality animal care program and follows state and federal Animal Welfare Acts, standards, and policies of the US Department of Health and Human Services. WFSM has an Assurance on file in the Office for Protection from Research Risks, Office of the Director, NIH, that accepts responsibility for the humane care and use of animals (OPRR #A-3391-01). The Laboratory Animal Care Program of the WFSM complies with the "Principles for Use of Animals," the "Guide for the Care and Use of Laboratory Animals" (47), all provisions of the Animal Welfare Act and is accredited by AAALAC.

Agent and Dosing. Synthetic TLR2/TLR6 binding diacyl lipopeptide (Pam2-CysGlyAspProLysHisProLysSerPhe) was obtained from Invivogen, synthesized in large quantities as a VacciGrade endotoxin-free biomolecule. The agent, Fibroblast Stimulating Ligand or FSL-1, dissolves rapidly in PBS, is stored at 4 °C, and is protected from light. Dosing in mice was based on previous work (7) and through empirical determination. Dose selection for subcutaneous administration to NHP was based on FDA guidelines for human equivalency dosing (20). Each NHP was administered a single subcutaneous dose of 0.09 mg/kg (7.0 to 12.8 mL) FSL-1 or saline Vehicle control 24 h after irradiation.

Radiation. Unanesthetized mice were placed in a silicone pie irradiator cage, positioned into the GammaCell 40 Exactor (Best Theratronics Ltd.), and given 5, 7.5, or 8.2 Gy TBI at a dose rate of 0.88 Gy/min. Biodosimetry was confirmed using phantoms such that delivered dose was 102% of targeted dose, as performed by an external radiation calibration laboratory (K. Kunugi, Medical Radiation Research Center, University of Wisconsin). The mice were monitored for ARS where clinical parameters encompassed weight loss, body temperature change, dehydration, hunching posture, reduced activity, increased respiration rate and/or effort, piloerection, change in grooming, and change in appetite, with no supportive care provided.

Irradiation methods, supportive care strategies, and analyses of acute effects provided a framework to test FSL-1 mitigation in NHPs (48–50). NHPs were anesthetized with ketamine (5 to 15 mg/kg sc) and dexmedetomidine (0.0075 to 0.015 mg/kg sc) for irradiation. NHPs received TBI in a single fraction of 4 Gy midplane according to the radiation protocol of 6MV X-rays using parallel-opposed lateral fields, 0.8 Gy/min at midplane. All irradiations were performed using an Elekta AB, calibrated using a national standard for clinical radiation dosimetry. The NHP research radiation protocol was validated using phantom and ionization chamber measurements on the day of irradiation, prior to experimental NHP irradiation. Transit biodosimetry using ionization chamber measurements was then performed for each subject to confirm the delivered dose to each individual NHP.

Health Monitoring of NHP. All NHPs were monitored twice daily by the veterinary staff to assure animal well-being and social stability. Clinical evaluations to monitor changes in weight, bruising, and stool consistency were performed and ranked to assess signs of illness, hematologic failure, or infection using NHP-specific modifications of the Children's Cancer Group Clinical Toxicity Criteria (51). Any NHPs with clinical concerns were promptly evaluated by institutional clinical veterinarians independent of the research team. Physical handling of the NHP was limited to avoid bruising. No antibiotics were provided to reduce additional disruption of gastrointestinal microbiome homeostasis. NHP consumed a diet of laboratory chow (Purina LabDiet Monkey Diet 5038) that was supplemented with fresh fruits and vegetables and given access to water ad libitum. They were housed socially in group cages. Care was taken to ensure that the animals in the groups were compatible. Environmental enrichment, including fruits/vegetables, toys, puzzles, climbing, and hiding environments, was provided continuously on a rotating basis. Recommendations regarding behavioral well-being were made as needed by an independent behavioral management team. Sampling was scheduled so that the animals were sedated a minimum number of times required for sample collection.

Peripheral Blood Clinical Chemistry. To assess hematologic and immunologic recovery after radiation, NHPs were sedated with intramuscular ketamine, and blood was drawn from the femoral vein for complete blood counts (CBCs), including hematocrit, red blood cell (RBC) indices, total and differential leukocyte, hemoglobin, and platelet counts. Serum chemistries were determined using a standard animal clinical chemistry panel. CBC and serum chemistry profiles were performed at IDEXX Bioanalytics, North Grafton, MA. Peripheral blood samples were immunophenotyped by flow cytometry as described in *SI Appendix, Materials and Methods*, Fig. S6 and Table S1.

Bone Marrow Pathogenesis. BM samples were collected from mice before and after 5 Gy TBI on days 8 and 30. These cells were immunophenotyped by flow cytometry as described in *SI Appendix, Materials and Methods*, Fig. S2 and Table S1. Additionally, femurs from mice at day 8 after treatment were fixed in 10% neutral buffered formalin, embedded in paraffin (FFPE), sectioned, and examined by light microscopy. FFPE sections (5 μm) were subjected to deparaffinization, rehydration, and antigen retrieval (#ab93678, Abcam). Sections were blocked with 10% normal goat serum and probed with αKi67 antibody (#11-5698-82, 1:200 dilution, ThermoFisher) or TUNEL HRP-DAB assay kit (ab206386, Abcam) according to the manufacturer's protocols. Images of probed femur sections were acquired with a Keyence BZ-X710 microscope and quantified using ImageJ software.

BM aspirates were collected from NHP prior to radiation and at days 22 and 65 post-radiation using 18-gauge BM needles. Post-aspirate analgesics (buprenorphine or ketoprofen) were administered. BM samples were prepared as cytospins onto a glass slide after diluting the collected, RBC-lysed samples 10-fold to 30-fold in 4% fetal bovine serum (FBS)/phosphate-buffered saline (PBS). Excess marrow cells were resuspended in 90% FBS/10% dimethyl sulfoxide (DMSO) and frozen in liquid nitrogen for downstream molecular analysis. The Diff-Quik (Romanowsky) stained slides were examined by a veterinary pathologist (D.L.C.) in a blind fashion. The relative subjective assessment of cellularity included "2" as normocellular or baseline, "1" as hypocellular or radiation-injured, and "3" as hypercellular or radiation-recovered. Further, each slide was evaluated for the relative presence of each cell lineage (i.e., neutrophil, lymphocyte, etc.) and scored according to a semiquantitative scale of 0 (none) to 3 (abundant).

Transcript Biomarker Analysis. RNA was extracted from mouse BM cells using the RNEasy Kit according to the manufacturer's protocol (Qiagen). Transcripts were measured by qPCR analyses using universal SYBR green super-mix reagent (Bio-Rad) and QuantStudio 6 Flex real-time PCR system (Thermo Fisher). Results were normalized to *Actb* expression. Gene expression for *Tlr2* and *Mmp9* was determined by the ΔΔCt method (2-ΔΔCt).

RNA derived from cryopreserved NHP BM was profiled using nCounter® Pro Analysis System (NanoString) (34). Multiplexed capture and reporter probes including positive and negative controls specific for rhesus macaque transcripts were mixed with 185 ng of purified mRNA per the manufacturer's instructions. The mixture was hybridized in a thermal cycler (Eppendorf) for 18 h at 65 °C. Following mix and wash steps, transcripts were quantified. Differentially expressed genes were normalized by processing to negative control genes as described (*SI Appendix, Materials and Methods* and Table S2).

Statistical Analysis. All graphics were produced using GraphPad Prism (version 9). Statistical analyses were conducted using the R statistical environment (52) (version 4.2.2) along with extension packages from the Comprehensive R Archive Network (CRAN), unless noted otherwise. Functions from the R stats package were used for inferential analyses. The reported *P* values were not adjusted for multiple testing unless otherwise specified. The analyses were carried out with adherence to the principles of reproducible analysis using RMARKDOWN (53) (version 2.19) and KNITR (54) packages (version 1.41) for generation of dynamic reports. Claims of differences between groups were based on an unadjusted *P* value cutoff at 0.05. Details of statistical analyses are summarized in *SI Appendix, Materials and Methods* and Table S3.

Data, Materials, and Software Availability. Analyses were conducted in accordance with the principles of reproducible analysis using Duke's Office of Information Technology GitLab (https://gitlab.oit.duke.edu/dcibioinformatics/pubs/pnas-brickey-etal-2023) for source code management. The R codes for replicating the statistical analyses presented here have been made accessible through a public source code repository (IMMPORT at https://immport.niaid.nih.gov). All statistical approaches applied are listed in *SI Appendix,* Table S3. All data are included in the manuscript and/or *SI Appendix*.

ACKNOWLEDGMENTS. We are grateful for the important contributions from Center for Medical Countermeasures Research colleagues (Drs. Julian Whitelegge and Ke Sheng at University of California at Los Angeles, Keith Kunugi at the University of Wisconsin) and Dr. Martin Hsu (The University of North Carolina at Chapel Hill) for guidance in quantification of murine biomarkers using ImageJ. This work was supported by the National Institute of Allergy and Infectious Diseases National Institutes of Health (NIH) U19 AI067798, NIH U19 AI067773(GG014746-22) (H.G.), and by the Department of Defense Congressionally Directed Medical Research Program grant W81XWH-15-1-0574 (J.M.C.). Multiplex cytokine profiling was performed in the Duke Regional Biocontainment Laboratory, which received partial support for construction from the NIH/National Institute of Allergy and Infectious Disease (UC6AI058607; G.D.S.). Flow cytometry was performed in Duke Human Vaccine Institute Flow Cytometry Facility. Multiplexed transcript analysis was performed in the Comparative Pathology Laboratory in the Section on Comparative Medicine, Department of Pathology, which is supported in part by an National Cancer Institute Cancer Center Support Grant (P30CA012197) (D.L.C.) to the Comprehensive Cancer Center of Wake Forest Baptist Medical Center. The funders had no role in data collection and analysis, decision to publish, or preparation of the manuscript.

Author affiliations: [a]Department of Microbiology and Immunology, University of North Carolina at Chapel Hill, Chapel Hill, NC 27599; [b]Lineberger Comprehensive Cancer Center, Center of Translational Immunology, University of North Carolina at Chapel Hill, Chapel Hill, NC 27599; [c]Department of Pathology, Section on Comparative Medicine, Wake Forest University School of Medicine, Winston Salem, NC 27157; [d]Duke Human Vaccine Institute, Department of Medicine, Duke University School of Medicine, Durham, NC 27710; [e]Department of Biostatistics and Bioinformatics, Duke University School of Medicine, Durham, NC 27705; [f]Department of Genetics, University of North Carolina at Chapel Hill, Chapel Hill, NC 27599; [g]Department of Radiation Oncology, Wake Forest University School of Medicine, Winston Salem, NC 27157; [h]Department of Biostatistics and Data Science, Wake Forest University School of Medicine, Winston Salem, NC 27157; [i]Department of Pharmacology, University of North Carolina at Chapel Hill, Chapel Hill, NC 27599; [j]Duke Cancer Institute, Department of Biostatistics and Bioinformatics, Duke University School of Medicine, Durham, NC 27705; and [k]Department of Medicine, Duke University School of Medicine, Durham, NC 27705

Author contributions: W.J.B., D.L.C., A.N.M., J.D.O., J.M.C., and J.P.Y.T. designed research; W.J.B., D.L.C., A.N.M., J.D.O., S.L., G.O.D., J.D.B., L.M.O., J.A.T., G.H., S.Y., H.G., M.N.F., and A.N.S. performed research; W.J.B., D.L.C., A.N.M., A.N.S., W.C.Z., G.D.S., N.J.C., and J.M.C. contributed new reagents/analytic tools; W.J.B., D.L.C., A.N.M., J.D.O., Y.D., Z.L., and K.O. analyzed data; and W.J.B., D.L.C., A.N.M., J.D.O., Y.D., J.M.C., and J.P.Y.T. wrote the paper.

Competing interest statement: J.P.Y.T. is a cofounder of and stockholder in IMMvention Therapeutix, which is developing inflammasome inhibitors. US20200282006A1 United States Methods and treatments using toll-like receptor agonists to mitigate hematopoietic myeloid loss, increase gastrointestinal recovery and reduce tumor growth for J.P.Y.T., W.J.B., and H.G.

This article is a PNAS Direct Submission. J.S.G. is a guest editor invited by the Editorial Board.

1. A. M. Farese, T. J. MacVittie, Filgrastim for the treatment of hematopoietic acute radiation syndrome. *Drugs Today (Barc)* **51**, 537–548 (2015).
2. A. F. McGettrick, L. A. O'Neill, Toll-like receptors: Key activators of leucocytes and regulator of haematopoiesis. *Br J. Haematol.* **139**, 185–193 (2007).
3. L. G. Burdelya *et al.*, An agonist of toll-like receptor 5 has radioprotective activity in mouse and primate models. *Science* **320**, 226–230 (2008).
4. M. Vijay-Kumar *et al.*, Flagellin treatment protects against chemicals, bacteria, viruses, and radiation. *J. Immunol.* **180**, 8280–8285 (2008).
5. F. Gao *et al.*, A critical role of toll-like receptor 2 (TLR2) and its' in vivo ligands in radio-resistance. *Sci. Rep.* **5**, 13004 (2015).
6. Z. Liu *et al.*, Toll-like receptors and radiation protection. *Eur. Rev. Med. Pharmacol. Sci.* **22**, 31–39 (2018).
7. C. J. Kurkjian *et al.*, The toll-like receptor 2/6 agonist, FSL-1 lipopeptide, therapeutically mitigates acute radiation syndrome. *Sci. Rep.* **7**, 17355 (2017).
8. B. J. Chen *et al.*, Growth hormone mitigates against lethal irradiation and enhances hematologic and immune recovery in mice and nonhuman primates. *PLoS One* **5**, e11056 (2010).
9. C. E. Bryant, T. P. Monie, Mice, men and the relatives: Cross-species studies underpin innate immunity. *Open Biol.* **2**, 120015 (2012).
10. C. Vaure, Y. Liu, A comparative review of toll-like receptor 4 expression and functionality in different animal species. *Front. Immunol.* **5**, 316 (2014).
11. H. Huhta *et al.*, The expression of toll-like receptors in normal human and murine gastrointestinal organs and the effect of microbiome and cancer. *J. Histochem. Cytochem.* **64**, 470–482 (2016).
12. C. Ketloy *et al.*, Expression and function of Toll-like receptors on dendritic cells and other antigen presenting cells from non-human primates. *Vet Immunol. Immunopathol.* **125**, 18–30 (2008).
13. D. Thierry-Mieg, J. Thierry-Mieg, AceView: A comprehensive cDNA-supported gene and transcripts annotation. *Genome Biol.* **7**, 11–14 (2006).
14. A. M. Farese, K. G. Hankey, M. V. Cohen, T. J. MacVittie, Lymphoid and myeloid recovery in rhesus macaques following total body X-irradiation. *Health Phys.* **109**, 414–426 (2015).
15. V. K. Singh, V. L. Newman, A. N. Berg, T. J. MacVittie, Animal models for acute radiation syndrome drug discovery. *Expert Opin. Drug Discov.* **10**, 497–517 (2015).
16. W. R. Hanson *et al.*, Comparison of intestine and bone marrow radiosensitivity of the BALB/c and the C57BL/6 mouse strains and their B6CF1 offspring. *Radiat. Res.* **110**, 340–352 (1987).
17. B. Ponnaiya, M. N. Cornforth, R. L. Ullrich, Radiation-induced chromosomal instability in BALB/c and C57BL/6 mice: The difference is as clear as black and white. *Radiat. Res.* **147**, 121–125 (1997).
18. A. C. Herman *et al.*, Systemic TLR2 agonist exposure regulates hematopoietic stem cells via cell-autonomous and cell-non-autonomous mechanisms. *Blood Cancer J.* **6**, e437 (2016).
19. A. Chow *et al.*, Bone marrow CD169+ macrophages promote the retention of hematopoietic stem and progenitor cells in the mesenchymal stem cell niche. *J. Exp. Med.* **208**, 261–271 (2011).
20. A. B. Nair, S. Jacob, A simple practice guide for dose conversion between animals and human. *J. Basic Clin. Pharm* **7**, 27–31 (2016).
21. V. I. Krivokrysenko *et al.*, The toll-like receptor 5 agonist entolimod mitigates lethal acute radiation syndrome in non-human primates. *PLoS One* **10**, e0135388 (2015).
22. M. Drouet *et al.*, Single administration of stem cell factor, FLT-3 ligand, megakaryocyte growth and development factor, and interleukin-3 in combination soon after irradiation prevents nonhuman primates from myelosuppression: Long-term follow-up of hematopoiesis. *Blood* **103**, 878–885 (2004).
23. A. N. Shakhov *et al.*, Prevention and mitigation of acute radiation syndrome in mice by synthetic lipopeptide agonists of Toll-like receptor 2 (TLR2). *PLoS One* **7**, e33044 (2012).
24. V. K. Singh *et al.*, CBLB613: A TLR 2/6 agonist, natural lipopeptide of Mycoplasma arginini, as a novel radiation countermeasure. *Radiat. Res.* **177**, 628–642 (2012).
25. D. Zhou *et al.*, Effects of NF-kappaB1 (p50) targeted gene disruption on ionizing radiation-induced NF-kappaB activation and TNFalpha, IL-1alpha, IL-1beta and IL-6 mRNA expression in vivo. *Int. J. Radiat Biol.* **77**, 763–772 (2001).
26. V. K. Singh, R. L. Shafran, C. E. Inal, W. E. Jackson III, M. H. Whitnall, Effects of whole-body gamma irradiation and 5-androstenediol administration on serum G-CSF. *Immunopharmacol. Immunotoxicol.* **27**, 521–534 (2005).
27. V. I. Krivokrysenko *et al.*, Identification of granulocyte colony-stimulating factor and interleukin-6 as candidate biomarkers of CBLB502 efficacy as a medical radiation countermeasure. *J. Pharmacol. Exp. Ther* **343**, 497–508 (2012).
28. N. J. Laping *et al.*, TLR2 agonism reverses chemotherapy-induced neutropenia in Macaca fascicularis. *Blood Adv.* **1**, 2553–2562 (2017).
29. J. Du *et al.*, Zymosan-a protects the hematopoietic system from radiation-induced damage by targeting TLR2 signaling pathway. *Cell Physiol. Biochem.* **43**, 457–464 (2017).

30. P. Autissier, C. Soulas, T. H. Burdo, K. C. Williams, Immunophenotyping of lymphocyte, monocyte and dendritic cell subsets in normal rhesus macaques by 12-color flow cytometry: Clarification on DC heterogeneity. *J. Immunol. Methods* **360**, 119–128 (2010).
31. I. Messaoudi, R. Estep, B. Robinson, S. W. Wong, Nonhuman primate models of human immunology. *Antioxid. Redox Signal* **14**, 261–273 (2011).
32. C. M. Brackett *et al.*, Signaling through TLR5 mitigates lethal radiation damage by neutrophil-dependent release of MMP-9. *Cell Death Discov.* **7**, 266 (2021).
33. R. Ahmad, P. K. Shihab, S. Jasem, K. Behbehani, FSL-1 induces MMP-9 production through TLR-2 and NF-κB /AP-1 signaling pathways in monocytic THP-1 cells. *Cell Physiol. Biochem.* **34**, 929–942 (2014).
34. NanoString Technologies Inc., nCounter® Analysis System Grant Application Package [Brochure]. Nanostring Technologies. https://nanostring.com/wp-content/uploads/2023/03/BR_MK4429_nCounter_Brochure_r10.pdf. Accessed 1 September 2023.
35. Y. Chen *et al.*, Radioprotective effects of heat-killed mycobacterium tuberculosis in cultured cells and radiosensitive tissues. *Cell Physiol. Biochem.* **40**, 716–726 (2016).
36. D. N. Hu *et al.*, Toll-like receptor 2 and 6 agonist fibroblast-stimulating lipopeptide increases expression and secretion of CXCL1 and CXCL2 by uveal melanocytes. *Exp. Eye Res.* **216**, 108943 (2022).
37. I. Koren Carmi, R. Haj, H. Yehuda, S. Tamir, A. Z. Reznick, The role of oxidation in FSL-1 induced signaling pathways of an atopic dermatitis model in HaCaT keratinocytes. *Adv. Exp. Med. Biol.* **849**, 1–10 (2015).
38. J. Nakamura *et al.*, Signaling pathways induced by lipoproteins derived from Mycoplasma salivarium and a synthetic lipopeptide (FSL-1) in normal human gingival fibroblasts. *Microbiol. Immunol.* **46**, 151–158 (2002).
39. S. Li, J. C. Yao, J. T. Li, A. P. Schmidt, D. C. Link, TLR7/8 agonist treatment induces an increase in bone marrow resident dendritic cells and hematopoietic progenitor expansion and mobilization. *Exp. Hematol.* **96**, 35–43.e37 (2021).
40. J. Megías *et al.*, Direct Toll-like receptor-mediated stimulation of hematopoietic stem and progenitor cells occurs in vivo and promotes differentiation toward macrophages. *Stem. Cells* **30**, 1486–1495 (2012).
41. T. Taylor, Y. J. Kim, X. Ou, W. Derbigny, H. E. Broxmeyer, Toll-like receptor 2 mediates proliferation, survival, NF-kappaB translocation, and cytokine mRNA expression in LIF-maintained mouse embryonic stem cells. *Stem. Cells Dev.* **19**, 1333–1341 (2010).
42. L. G. Schuettpelz *et al.*, G-CSF regulates hematopoietic stem cell activity, in part, through activation of Toll-like receptor signaling. *Leukemia* **28**, 1851–1860 (2014).
43. M. Takehara, S. Seike, T. Takagishi, K. Kobayashi, M. Nagahama, Peptidoglycan accelerates granulopoiesis through a TLR2- and MyD88-dependent pathway. *Biochem. Biophys. Res. Commun.* **487**, 419–425 (2017).
44. V. Redecke *et al.*, Cutting edge: Activation of Toll-like receptor 2 induces a Th2 immune response and promotes experimental asthma. *J. Immunol.* **172**, 2739–2743 (2004).
45. B. Schaub *et al.*, TLR2 and TLR4 stimulation differentially induce cytokine secretion in human neonatal, adult, and murine mononuclear cells. *J. Interferon Cytokine Res.* **24**, 543–552 (2004).
46. S. Agrawal, S. Gupta, TLR1/2, TLR7, and TLR9 signals directly activate human peripheral blood naive and memory B cell subsets to produce cytokines, chemokines, and hematopoietic growth factors. *J. Clin. Immunol.* **31**, 89–98 (2011).
47. National Research Council (US) Committee for the Update of the Guide for the Care and Use of Laboratory Animals. *Guide for the Care and Use of Laboratory Animals* (National Academies Press (US) Copyright © 2011, National Academy of Sciences, Washington (DC), ed. 8, 2011), 10.17226/12910.
48. A. M. Farese *et al.*, A nonhuman primate model of the hematopoietic acute radiation syndrome plus medical management. *Health Phys.* **103**, 367–382 (2012).
49. T. J. MacVittie, A. M. Farese, W. Jackson III, The hematopoietic syndrome of the acute radiation syndrome in rhesus macaques: A systematic review of the lethal dose response relationship. *Health Phys.* **109**, 342–366 (2015).
50. J. Z. Yu *et al.*, Subject-based versus population-based care after radiation exposure. *Radiat. Res.* **184**, 46–55 (2015).
51. F. M. Uckun *et al.*, Pharmacokinetic features, immunogenicity, and toxicity of B43(anti-CD19)-pokeweed antiviral protein immunotoxin in cynomolgus monkeys. *Clin. Cancer Res. J. Am. Assoc. Cancer Res.* **3**, 325–337 (1997).
52. R. Core Team, R: A language and environment for statistical computing (version 2022). R Foundation for Statistical Computing, Vienna, Austria. https://www.R-project.org/. Accessed 1 September 2023.
53. Y. Xie, J. J. Allaire, G. Grolemund, *R Markdown: The Definitive Guide* (Chapman and Hall/CRC, ed. 1, 2018).
54. Y. Xie, *Dynamic Documents with R and Knitr* (Chapman and Hall/CRC, ed. 2, 2015).